Journal of Integrated Knowledge
Vol. 2 No. 7 (2026)

Common Flight Phase and Individual Obstacle Geometry in a Ten-Drone Formation Record

Mark Griffin[1] · Alexander Johnston[2] · Jason Reed[3]

[1] Lithuania · [2] Iceland · [3] Luxembourg

Published: July 08, 2026 | Article 860

Abstract

A swarm can simultaneously move farther from obstacles and closer to its assigned formation, creating a pooled association that partly reflects shared flight phase. We examined this distinction in one public ten-drone formation record. An integer-clock interpolation protocol retained 1,889 contiguous 10 Hz ticks, yielding 18,890 agent observations. The pooled formation-deviation slope against recorded external-obstacle clearance was −1.5218 m/m; removing agent and tick effects produced −0.7497 m/m, with a lag-50 Bartlett time-HAC working 95% interval of −0.9041 to −0.5953. All ten agent-omission slopes remained negative. However, the fitted norm was negative in 387 pooled and 2,046 adjusted observations. The record supports a conditional geometric association while exposing the limitations of a linear summary; it does not identify obstacle-induced behavior, physical safety, or learning-controller performance.

Common Flight Phase and Individual Obstacle Geometry in a Ten-Drone Formation Record

Abstract

A swarm can simultaneously move farther from obstacles and closer to its assigned formation, creating a pooled association that partly reflects shared flight phase. We examined this distinction in one public ten-drone formation record. An integer-clock interpolation protocol retained 1,889 contiguous 10 Hz ticks, yielding 18,890 agent observations. The pooled formation-deviation slope against recorded external-obstacle clearance was -1.5218 m/m; removing agent and tick effects produced -0.7497 m/m, with a lag-50 Bartlett time-HAC working 95% interval of -0.9041 to -0.5953. All ten agent-omission slopes remained negative. However, the fitted norm was negative in 387 pooled and 2,046 adjusted observations. The record supports a conditional geometric association while exposing the limitations of a linear summary; it does not identify obstacle-induced behavior, physical safety, or learning-controller performance.

Introduction

Formation flight combines a collective arrangement with trajectories that each vehicle must execute in its immediate surroundings. A team may encounter narrow environmental geometry while its preferred shape changes, and an individual vehicle may deviate from an assigned reference without the team losing coordinated motion. The source system explicitly combines formation expectations and navigation through obstacles in an optimization-based platform (Zhou et al., 2022). Cooperative control also spans coordination, task allocation and trajectory planning, rather than a single scalar measure of team quality (Murray, 2007). Consequently, an observed correspondence between obstacle distance and formation error needs an explicit unit of comparison.

The formation-control literature distinguishes several ways of representing and controlling relationships among agents, making the definition of formation deviation consequential (Oh et al., 2015). Environmental proximity supplies a different geometric quantity. Potential-field obstacle avoidance uses environmental geometry in constructing control actions (Khatib, 1986), whereas navigation-function results connect geometric free space and feedback under stated assumptions (Rimon and Koditschek, 1992). These studies motivate attention to geometry but do not turn a recorded clearance field into a measured control command or a verified guarantee. Here, the observable is the source's distance to its nearest represented external obstacle.

Dynamics and planning further limit what that scalar can establish. The dynamic-window approach searches feasible velocity commands using robot dynamics (Fox et al., 1997); its decision problem contains information absent from a clearance-deviation regression. Motion-planning formulations also distinguish the physical arrangement of objects from configurations that a robot can reach (Latombe, 1991). LaValle (2006) treats geometric representations, sensing uncertainty and differential constraints as separate planning ingredients. We therefore analyze two recorded measurements without importing a planner's feasibility conditions, actuator model or obstacle guarantees into their statistical association.

A related evaluation distinction appears in learning-based flocking. The formal abstract of Guo et al. (2023) describes cooperative rewards alongside individual fitness and evolutionary selection. That bounded source supports keeping individual and collective criteria conceptually distinct; it supplies neither this experiment's controller nor an external-obstacle measurement model. This distinction motivates the present question: after removing stable agent differences and changes shared at a recorded

time, does the individual clearance-deviation association remain, and how does it differ from the pooled association? No learning algorithm is trained or evaluated to answer it.

Two descriptive propositions organize the frozen comparisons. P1 estimates the individual clearance-deviation association after agent and recorded-tick effects. P2 estimates the pooled association on identical observations and compares its magnitude with P1. Shared flight progression can affect both measurements, providing a reason these projections may differ. The acquired literature does not determine either coefficient's sign, and the protocol did not require a sign reversal or a particular magnitude difference. These propositions concern measurable associations rather than a tested control mechanism.

Formation navigation among obstacles has also been formulated through distributed geometric and optimization procedures with reconfiguration (Alonso-Mora et al., 2016). In contrast, reciprocal collision-avoidance formulations concern interactions among moving agents (van den Berg et al., 2011). That distinction prevents us from equating environmental clearance with inter-vehicle separation. Distributed behavioral flocking models (Reynolds, 1987) and dynamical flocking theory (Olfati-Saber, 2006) likewise concern collective organization; an individual assigned-reference norm does not alone establish their collective properties. The contribution here is a measured pooled-versus-conditional comparison within one full formation record, rather than an implementation of those methods.

Data and measurement

We used the complete twenty acquired numeric CSV members for the ten-agent formation experiment in the public Version 1 dataset released on 25 December 2021 (Zhou et al., 2021). Ten corrected-odometry files contain 376,932 rows; ten corresponding formation-error files contain another 376,932 rows at exactly matching same-agent timestamps. These paired channels describe one recorded flight. They are not independent replications, and the combined 753,864 source rows are not the analysis sample size. The provider declares GPL-2.0. Selected members were acquired on 16 November 2026 using archive range reads, and each member's size and CRC32 matched the archive directory. The entire archive was not downloaded, so its provider whole-file MD5 remains unverified. Local member SHA256 hashes and acquisition details accompany the analysis.

The source README defines formation error as corrected odometry minus the formation target position and identifies the odometry distance field as distance to the nearest obstacle. We use metres for both clearance and error. The response E is the Euclidean norm of the three recorded formation-error components after interpolation. The predictor D is interpolated recorded nearest-obstacle clearance. Measurement interpretation matters: a numerical operation does not itself establish that its result represents the intended physical construct (Hand, 2004). E refers to the source's assigned, potentially moving reference; D refers to the source's environmental representation. Neither is an independent survey of physical truth.

All required source values are finite, and native times strictly increase. Six-decimal source timestamps were parsed exactly into integer microseconds. The common ten-agent interval is 1630221242415099-1630221431332041 microseconds, lasting 188.916942 seconds. Exact serialization and matched channel timestamps establish computational alignment on the recorded clock. They do not authenticate cross-vehicle clock accuracy or remove localization error. Both E and D depend on corrected position, so common estimation errors and geometric construction can contribute to their association. The analysis does not estimate that contribution separately.

Before coefficient estimation, we froze an absolute grid with 100,000-microsecond spacing, starting at the first grid tick at or above the common start and ending strictly before the common end. An exact native

timestamp is supported directly. Otherwise, linear interpolation requires bracketing native rows no more than 20,000 microseconds apart; there is no extrapolation. We interpolated the three error components before taking their norm. Interpolating native norms would produce a different response because a norm is nonlinear. Every interpolation index, span, weight and support flag is retained for inspection.

The protocol selects the longest contiguous run supported by every agent, resolving equal-length ties by the earlier run. Both models use that same run. This rule protects the equally spaced interpretation of time lags; it does not compress supported observations across missing intervals. In the realized data, all 1,889 candidate ticks were supported by all ten agents, so no candidate tick was removed. The first and last grid times are 1630221242500000 and 1630221431300000 microseconds, separated by 188.8 seconds. The resulting panel has 18,890 observations with equal agent representation.

We retained the full common record without selecting flight phases, clearance thresholds, outcome outliers or preferred agents. The auxiliary nearest-obstacle coordinate tuple is all zero in some native rows, but the acquired documentation does not establish that this invalidates the distance field. Fifteen selected agent-tick observations have an interpolation bracket touching such a tuple; all remain included. This unresolved auxiliary-field issue is a source limitation, not an empirically chosen exclusion. Recorded positive clearance is never relabeled a safe margin or a verified absence of collision.

Analysis model and uncertainty

The primary model is $E_{it} = \alpha_i + \gamma_t + \beta_{within} D_{it} + u_{it}$, with an agent effect for each drone and a recorded-tick effect for each common time. The pooled comparator is $E_{it} = \alpha + \beta_{pooled} D_{it} + v_{it}$ on identical observations. Agent effects remove persistent additive differences; tick effects remove additive changes common to the team. Panel methods make such distinctions explicit (Wooldridge, 2010), and pooling repeated units requires attention to their unit-specific effects (Mundlak, 1978). Neither adjustment makes clearance externally assigned or converts the resulting coefficient into a causal response.

For the balanced panel, we computed $X_{it} = D_{it} - \text{mean}_i(D) - \text{mean}_t(D) + \text{grand_mean}(D)$, and the analogous Y for E. The coefficient is $\Sigma XY/\Sigma X^2$, following the partial-regression principle associated with Frisch and Waugh (1933). Lovell (1963) extends the connection between preliminary least-squares adjustment and including corresponding regressors. Here the projection is exact double centering, rather than an estimated smoother. We checked its agent and tick means, the residual centering identities and the slope normal equation. The pooled fit uses its full intercept-and-clearance design.

PPO-Exp gives a second, distinct formation-evaluation motivation. Its published discussion assembles individual formation terms within a joint task objective and includes separate task or stopping concerns (Xu et al., 2023). This makes it useful to distinguish a local geometric association from a pooled team summary. Its inter-UAV collision discussion does not establish handling of the external-obstacle field used here. The current ten-drone source used a different optimization-based system. We do not execute PPO-Exp, reproduce its reward equation, evaluate fixed-wing performance or transfer its reported results to this flight.

Figure 1 links P1 and P2 to their shared measurement support and separate regression terms. Its shared-position annotation also records a measurement dependency that neither statistical projection resolves. Thus, the diagram defines the comparison and its limits rather than proposing a causal pathway from clearance to control behavior.

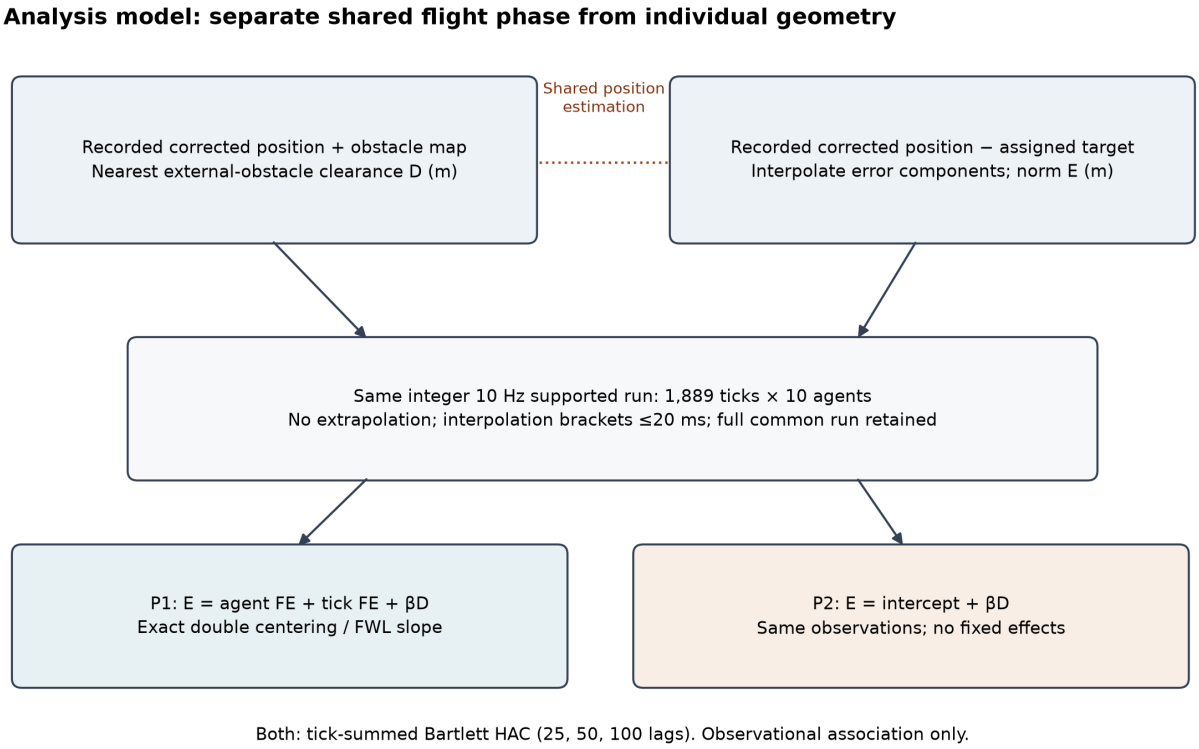

Figure 1. Study-specific analysis model. Arrows indicate data processing and model inputs, not causal effects. The dotted connection records the shared corrected-position dependence of clearance and formation deviation. The same supported interval supplies both fitted models.

All agents at a tick can be dependent. We therefore sum their regression scores at each tick before calculating heteroskedasticity-and-autocorrelation-consistent uncertainty. For the within model, $s_t = \Sigma_i X_{it} u_{it}$. The Bartlett meat is $\Sigma_t s_t^2 + 2\Sigma_l w_l \Sigma_t s_t s_{t-l}$, where $w_l = 1-l/(L+1)$. Dividing by $(\Sigma X^2)^2$ yields the slope variance. The pooled model uses its full two-dimensional tick-summed score and bread matrix. This follows the time-HAC construction of Newey and West (1987), with no additional finite-sample multiplier. Individual agent rows are never treated as independent time replicates.

The primary bandwidth is 50 ticks, corresponding to five seconds of grid spacing. We also report the predeclared 25- and 100-tick bandwidths in full. Kernel and truncation choices affect HAC covariance estimation (Andrews, 1991); none was selected by the interval most favorable to a claim. Normal 95% intervals are conditional working summaries for this record. Their calculation does not resolve nonstationarity, validate the linear mean model or represent uncertainty across flights. The separation of scores, bread and covariance also supports computational auditing (Zeileis, 2004); no R package was used.

We additionally omitted each entire agent once and refitted the within model on the other nine agents at all retained ticks. These ten fixed composition diagnostics are deterministic refits, not confidence intervals or independent experiments. Rank failures, insufficient support, negative or nonfinite variances and degenerate residual variation were to remain explicitly undefined. No alternative window, nonlinear model or bandwidth would replace an unfavorable result. These rules were frozen before outcome calculation. A later fitted-value diagnostic was documented separately and changed no sample, coefficient, covariance or primary analysis choice.

Results

On the retained grid, recorded clearance averaged 0.552880 m and ranged from 0.152499 to 2.094413 m. Formation-deviation norm averaged 0.734290 m and ranged from 0.001693 to 1.670123 m. These grid ranges differ from native-file extrema because interpolation and common support define the analysis observations. All ten agents contributed exactly 1,889 ticks. The within-clearance sum of squares was 183.183262 m², providing nondegenerate residualized variation. Centered residual means across agents and ticks were below 2.3×10^{-15} m in absolute value, consistent with the specified projections.

The pooled slope was -1.521786 m/m; the adjusted slope was -0.749699 m/m (Table 1). Thus, the negative association persisted after both additive adjustments, while its magnitude was substantially smaller. The pooled-minus-within point difference was -0.772087 m/m. We do not assign a causal interpretation or a separately tested uncertainty interval to that difference. Each coefficient answers a different descriptive question. A one-metre slope unit summarizes a linear projection across observed variation and should not be read as a feasible intervention or an individual drone's response over that entire range.

Table 1. Actual fitted associations on the identical full common run. Ordinary R² uses total deviation about the grand response mean. Within R² uses the double-centered response sum of squares. Their denominators differ, so these values do not rank the models' predictive performance. Intervals use tick-summed scores and describe conditional working time uncertainty for one flight.

Model	Observations / ticks / agents	Clearance slope, m/m	Lag-50 working SE	Working 95% interval	Reported R²
Pooled intercept + clearance	18,890 / 1,889 / 10	-1.521786	0.050325	[-1.620420, -1.423151]	0.803254 ordinary
Agent + recorded-tick effects	18,890 / 1,889 / 10	-0.749699	0.078762	[-0.904070, -0.595328]	0.252637 within

The pooled intercept was 1.575655 m, with residual sum of squares 1193.937440 m² and total sum of squares 6068.425226 m². The within residual sum of squares was 304.574259 m² against a double-centered response sum of squares of 407.532158 m². The pooled design had rank two, and the within clearance passed its numerical variation check. Both models and every planned HAC calculation were defined; no covariance was clipped, replaced or hidden. Lower residual variation after introducing many tick and agent effects is not independent evidence of generalization to a new trajectory.

Bandwidth sensitivity changed the working interval width while preserving the negative estimated association (Table 2). For the within model, the standard error increased from 0.067024 at 25 lags to 0.087265 at 100 lags. For the pooled fit, it increased from 0.038107 to 0.062685. These are all prescribed calculations rather than alternative selected analyses. All intervals excluded zero within this working construction, but that arithmetic result does not establish that its normal approximation adequately describes repeated flights or that unmeasured geometric dependence has been removed.

Table 2. All predeclared bandwidths. Coefficients and observations are fixed across these covariance calculations; 50 lags is primary.

Bartlett lags	Pooled slope SE	Pooled working 95% interval	Within slope SE	Within working 95% interval
25	0.038107	[-1.596474, -1.447097]	0.067024	[-0.881063, -0.618335]
50	0.050325	[-1.620420, -1.423151]	0.078762	[-0.904070, -0.595328]
100	0.062685	[-1.644646, -1.398925]	0.087265	[-0.920735, -0.578663]

Every nine-agent refit remained negative. Omitting agents 0-9 in order gave slopes of -0.653593, -0.740408, -0.749318, -0.750490, -0.737852, -0.773196, -0.761547, -0.762908, -0.775021 and -0.759657 m/m. Each refit contained 17,001 observations and 1,889 ticks. The complete range was [-0.775021, -0.653593] m/m. Omitting agent 0 changed the magnitude most strongly toward zero, but it did not reverse the sign. Keeping every omission visible prevents a favorable composition from replacing the ten-agent result.

Figure 2 places the full bandwidth results beside all ten omissions. The two displays answer different sensitivity questions: interval width concerns the working covariance construction, whereas the omission points concern team composition. Neither display adds independent flights or physical validation.

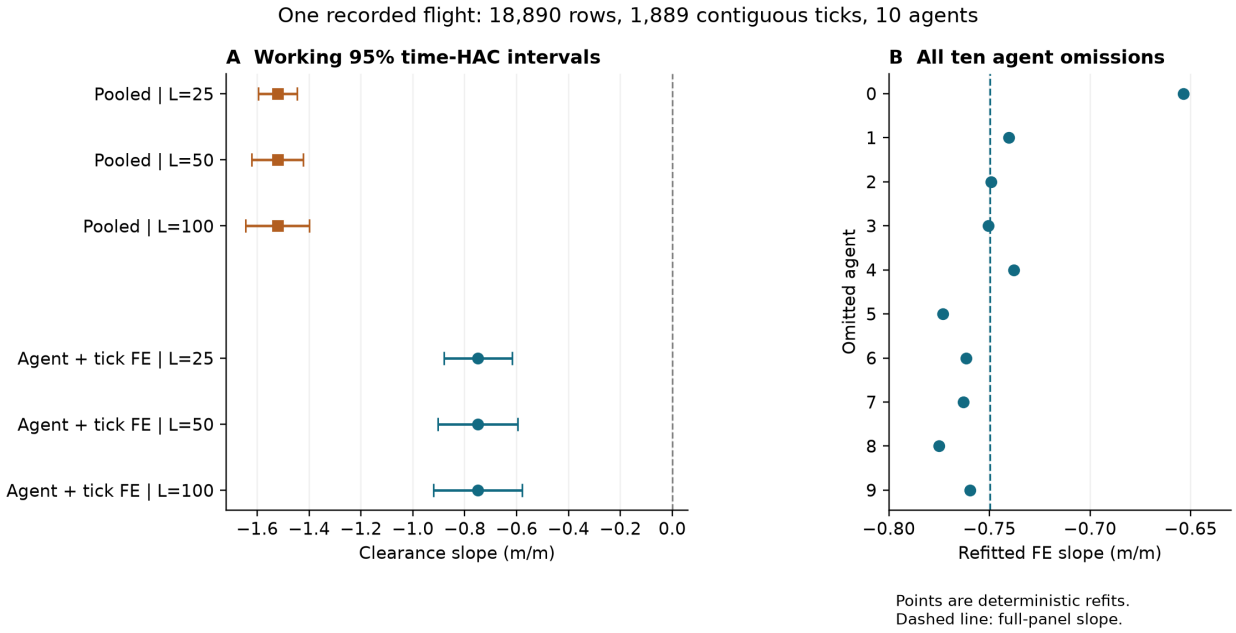

Figure 2. Panel A shows all actual slopes and conditional working 95% time-HAC intervals, using different symbols for the two models. Panel B shows every whole-agent omission; the dashed line is the full-panel within slope. Omission points have no confidence-interval interpretation. All panels summarize the same recorded flight.

The linear functional form had a material weakness. Although the response is a nonnegative norm, pooled fitted values ranged from -1.611593 to 1.343584 m and included 387 negative values. Reconstructed within-model fitted values, including their agent and tick components, ranged from -0.206461 to 1.679153 m and included 2,046 negative values. These were retained without truncation. The models summarize association but do not provide physically constrained predictions of deviation. Robust covariance estimation cannot repair an unsuitable mean specification or create the intended scientific interpretation (Freedman, 2006). No nonlinear replacement was fitted after observing this diagnostic.

Interpretation and reproducibility

The adjusted association shows that pooled common progression does not exhaust the measured clearance-deviation relationship under the stated additive projection. It does not isolate obstacle-induced avoidance. The moving assigned reference, shared corrected-position estimation, local map construction and unmeasured agent-specific dynamics can all influence the measurements. Additive time effects cannot remove every interaction between an agent and changing surroundings. Even the word clearance is operational: the acquired field records nearest represented external-obstacle distance, rather than a complete physical collision envelope, sensor uncertainty bound or control feasibility test.

This record contains only one flight under one source system. Ten simultaneous agents increase the available geometric contrasts but do not supply ten independent missions. The all-negative omission range establishes a limited composition property of this dataset; it does not establish robustness to another map, controller, formation assignment or clock alignment. The increasing HAC widths reveal sensitivity to the prescribed time horizon, while the negative fitted norms directly constrain predictive use. A subsequent study could preregister independently calibrated geometry and a nonnegative response model, but that would require new evidence and a separate design.

Computational reproducibility requires retaining the transformations that connect measurements to claims, not simply an executable fit (Peng, 2011). We retained all twenty source files, their integrity inventory, numeric provenance tables, frozen protocol, primary code and full precision results. Following the practical emphasis on traceable computational research in Sandve et al. (2013), the grid table includes support and interpolation information as well as centered variables and residuals. The independent checker reread raw CSV fields, used an advancing-pointer lookup instead of the primary array search, and recomputed the models through scalar sums without importing the primary fitting routine.

That independent reconstruction passed 171 scalar checks and 377,800 cell comparisons, including support, interpolation, centering, slopes, all HAC choices and every agent omission. Maximum absolute grid discrepancy was below 1.03×10^{-14} in the checked numeric fields. The main numerical implementation used Python 3.12.14 with NumPy 2.5.4 for array operations (Harris et al., 2020) and pandas 3.0.6 for numeric table handling (McKinney, 2010). Matplotlib 3.11.2 generated the figures (Hunter, 2007). The independent calculation used Python standard-library parsing and scalar arithmetic, which reduces shared implementation dependence without validating the source sensors.

Scientific-writing, statistical-analysis and scientific-visualization procedural skills guided provenance, reporting and figure review, with the actual library credited to Kassis et al. (2026). AI assistance produced code, draft prose and local consistency checks; accountable human source, claim and authorship review remains pending. No human investigator approval, new data collection, controller execution or submission is represented as completed. The retained evidence supports a negative conditional geometric association of smaller magnitude than its pooled counterpart, together with a concrete linear-model failure that must accompany any interpretation of that result.

Conclusion

In this one ten-drone record, the clearance-deviation association remained negative after removing stable agent offsets and changes shared at each recorded tick. The adjusted slope was substantially smaller in magnitude than the pooled slope, and every prescribed agent omission retained its sign. These findings distinguish individual relative geometry from pooled flight progression without isolating an avoidance mechanism. The negative fitted norms further show why neither linear projection should serve as a physically constrained prediction model. Claims about safety, other environments, controllers or reinforcement-learning performance require evidence beyond this record.

Declarations

This is an AI-assisted empirical manuscript draft. Accountable human source verification, claim approval, authorship, funding, competing-interest and submission declarations are PENDING. Public numeric data were processed locally; no private participant text, physical robot experiment or reinforcement-learning training was used. The recorded source license is GPL-2.0. Code, provenance, frozen protocol, full results, independent checks and figure sources are retained with this article. The accompanying review records distinguish local computational checks from accountable human scientific approval.

References

1. Mundlak, Yair. (1978). On the Pooling of Time Series and Cross Section Data. Econometrica. https://doi.org/10.2307/1913646
2. Reynolds, Craig W. (1987). Flocks, herds and schools: A distributed behavioral model. Proceedings of the 14th annual conference on Computer graphics and interactive techniques. https://doi.org/10.1145/37401.37406
3. Zhou, Xin; Wen, Xiangyong; Wang, Zhepei; Gao, Yuman; Li, Haojia; Wang, Qianhao; Yang, Tiankai; Lu, Haojian; Cao, Yanjun; Xu, Chao; Gao, Fei. (2022). Swarm of micro flying robots in the wild. Science Robotics. https://doi.org/10.1126/scirobotics.abm5954
4. McKinney, Wes. (2010). Data Structures for Statistical Computing in Python. Proceedings of the Python in Science Conference. https://doi.org/10.25080/majora-92bf1922-00a
5. Rimon, Elon; Koditschek, Daniel E. (1992). Exact robot navigation using artificial potential functions. IEEE Transactions on Robotics and Automation. https://doi.org/10.1109/70.163777
6. Alonso-Mora, Javier; Montijano, Eduardo; Schwager, Mac; Rus, Daniela. (2016). Distributed multi-robot formation control among obstacles: A geometric and optimization approach with consensus. 2016 IEEE International Conference on Robotics and Automation (ICRA). https://doi.org/10.1109/ICRA.2016.7487747
7. Wooldridge, Jeffrey M. (2010). Econometric Analysis of Cross Section and Panel Data. Second edition. MIT Press. https://mitpress.mit.edu/9780262232586/econometric-analysis-of-cross-section-and-panel-data/
8. Oh, Kwang-Kyo; Park, Myoung-Chul; Ahn, Hyo-Sung. (2015). A survey of multi-agent formation control. Automatica. https://doi.org/10.1016/j.automatica.2014.10.022
9. Frisch, Ragnar; Waugh, Frederick V. (1933). Partial Time Regressions as Compared with Individual Trends. Econometrica. https://doi.org/10.2307/1907330
10. Newey, Whitney K.; West, Kenneth D. (1987). A Simple, Positive Semi-Definite, Heteroskedasticity and Autocorrelation Consistent Covariance Matrix. Econometrica. https://doi.org/10.2307/1913610
11. LaValle, Steven M. (2006). Planning Algorithms. Cambridge University Press. https://doi.org/10.1017/CBO9780511546877
12. Harris, Charles R.; Millman, K. Jarrod; van der Walt, Stéfan J.; Gommers, Ralf; Virtanen, Pauli; Cournapeau, David; Wieser, Eric; Taylor, Julian; Berg, Sebastian; Smith, Nathaniel J.; Kern, Robert; Picus, Matti; Hoyer, Stephan; van Kerkwijk, Marten H.; Brett, Matthew; Haldane, Allan; Fernández del Río, Jaime; Wiebe, Mark; Peterson, Pearu; Gérard-Marchant, Pierre; Sheppard, Kevin; Reddy, Tyler; Weckesser, Warren; Abbasi, Hameer; Gohlke, Christoph; Oliphant, Travis E. (2020). Array programming with NumPy. Nature. https://doi.org/10.1038/s41586-020-2649-2.
13. Khatib, Oussama. (1986). Real-Time Obstacle Avoidance for Manipulators and Mobile Robots. The International Journal of Robotics Research. https://doi.org/10.1177/027836498600500106

14. Zhou, Xin; Wen, Xiangyong; Wang, Zhepei; Gao, Yuman; Li, Haojia; Wang, Qianhao; Yang, Tiankai; Lu, Haojian; Cao, Yanjun; Xu, Chao; Gao, Fei. (2021). Dataset - Swarm of Micro Flying Robots in the Wild. Zenodo dataset, version 1. https://doi.org/10.5281/zenodo.5804079

15. Freedman, David A. (2006). On The So-Called "Huber Sandwich Estimator" and "Robust Standard Errors". The American Statistician. https://doi.org/10.1198/000313006x152207

16. Peng, Roger D. (2011). Reproducible Research in Computational Science. Science. https://doi.org/10.1126/science.1213847

17. Murray, Richard M. (2007). Recent Research in Cooperative Control of Multivehicle Systems. Journal of Dynamic Systems, Measurement, and Control. https://doi.org/10.1115/1.2766721

18. Andrews, Donald W. K. (1991). Heteroskedasticity and Autocorrelation Consistent Covariance Matrix Estimation. Econometrica. https://doi.org/10.2307/2938229

19. Fox, Dieter; Burgard, Wolfram; Thrun, Sebastian. (1997). The dynamic window approach to collision avoidance. IEEE Robotics & Automation Magazine. https://doi.org/10.1109/100.580977

20. Kassis, Timothy; Agarwal, Vinayak; He, Yuhuan; Patel, Darshil; Brueckner, Aubrey M. (2026). Scientific Agent Skills: A Library of Procedural Knowledge for Research Agents. arXiv. https://doi.org/10.48550/arXiv.2609.00065

21. Xu, Dan; Guo, Yunxiao; Yu, Zhongyi; Wang, Zhenfeng; Lan, Rongze; Zhao, Runhao; Xie, Xinjia; Long, Han. (2023). PPO-Exp: Keeping Fixed-Wing UAV Formation with Deep Reinforcement Learning. Drones. https://doi.org/10.3390/drones7010028.

22. Zeileis, Achim. (2004). Econometric Computing with HC and HAC Covariance Matrix Estimators. Journal of Statistical Software. https://doi.org/10.18637/jss.v011.i10

23. Sandve, Geir Kjetil; Nekrutenko, Anton; Taylor, James; Hovig, Eivind. (2013). Ten Simple Rules for Reproducible Computational Research. PLoS Computational Biology. https://doi.org/10.1371/journal.pcbi.1003285

24. van den Berg, Jur; Guy, Stephen J.; Lin, Ming; Manocha, Dinesh. (2011). Reciprocal n-Body Collision Avoidance. Springer Tracts in Advanced Robotics. https://doi.org/10.1007/978-3-642-19457-3_1

25. Latombe, Jean-Claude. (1991). Robot Motion Planning. Springer. https://doi.org/10.1007/978-1-4615-4022-9

26. Guo, Yunxiao; Xie, Xinjia; Zhao, Runhao; Zhu, Chenglan; Yin, Jiangting; Long, Han. (2023). Cooperation and Competition: Flocking with Evolutionary Multi-Agent Reinforcement Learning. Lecture Notes in Computer Science. https://doi.org/10.1007/978-3-031-30105-6_23

27. Lovell, Michael C. (1963). Seasonal Adjustment of Economic Time Series and Multiple Regression Analysis. Journal of the American Statistical Association. https://doi.org/10.1080/01621459.1963.10480682

28. Hand, David J. (2004). Measurement Theory and Practice: The World Through Quantification. Wiley. https://www.wiley-vch.de/de/fachgebiete/mathematik-und-statistik/measurement-theory-and-practice-978-0-470-68567-9

29. Hunter, John D. (2007). Matplotlib: A 2D Graphics Environment. Computing in Science & Engineering. https://doi.org/10.1109/mcse.2007.55

30. Olfati-Saber, Reza. (2006). Flocking for Multi-Agent Dynamic Systems: Algorithms and Theory. IEEE Transactions on Automatic Control. https://doi.org/10.1109/tac.2005.864190